Lossy Image Compression with Filter Bank based Convolutional Networks

Shaohui Li*, Ziyang Zheng*, Wenrui Dai†, and Hongkai Xiong*

*Department of Electrical Engineering
Shanghai Jiao Tong University
Shanghai 200240, China
{lishaohui,doll001,xionghongkai}@sjtu.edu.cn

†School of Biomedical Informatics
University of Texas
Health Science Center at Houston
Houston, TX 77030, USA
wenrui.dai@uth.tmc.edu

Abstract

Filter bank based convolutional networks (FBCNs) enable efficient separable multiscale and multidirectional decomposition with a convolutional cascade of 1-D radial and directional filter banks. In this paper, we propose a two-stage subband coding framework for FBCN analysis coefficients using a SPIHT-like algorithm and subsequent primitive-based adaptive arithmetic coding (AAC). The SPIHT-like algorithm extends spatial orientation tree to exploit inter-subband dependency between subbands of different scales and directions. Mutual information is estimated for information-theoretical measurement to formulate such dependencies. Various primitives are designed adaptively encode the generated bitstream by fitting its varying lists and passes. Neural networks are leveraged to improve probability estimation for AAC, where nonlinear prediction is made based on contexts regarding scales, directions, locations and significance of analysis coefficients. Experimental results show that the proposed framework improves the lossy coding performance for FBCN analysis coefficients in comparison to the state-of-the-arts subband coding schemes SPIHT.

1 Introduction

Convolutional neural networks (CNNs) have been widely considered in a wide range of image processing tasks, including classification and recognition [1–3]. Despite its superior performance, it is not well understood for theoretical analysis due to cascaded non-linearities. Wavelet based convolutional networks like scattering network [4] are interpretable on well-established mathematical ground using a cascade of convolutions with wavelets and modules. Invariant scattering networks [5] were further extended by [6] into a generalized feature extractor based on semi-discrete frames and non-linearities. However, their approximation performances are degraded by high representation redundancies. As an improved alternative, perfect reconstruction filter banks were adopted to construct convolutional networks [7]. These networks partition the frequency domain of two-dimensional signals into multiscale and multidirectional subbands. Furthermore, extended conjugate polar Fourier transform (ECPFT) [8] enabled a separable realization based on 1-D radial and directional filter banks. These filter bank based convolutional networks (FBCNs) achieve efficient directional multiscale representations for image approximation.

Conventional image compression schemes leverage subband coding based on wavelet transform for compact image representation. Intra- and inter-subband dependencies are considered to exploit correlations among wavelet coefficients. For example, SPIHT

2375-0359/19/$31.00 ©2019 IEEE
DOI 10.1109/DCC.2019.00010

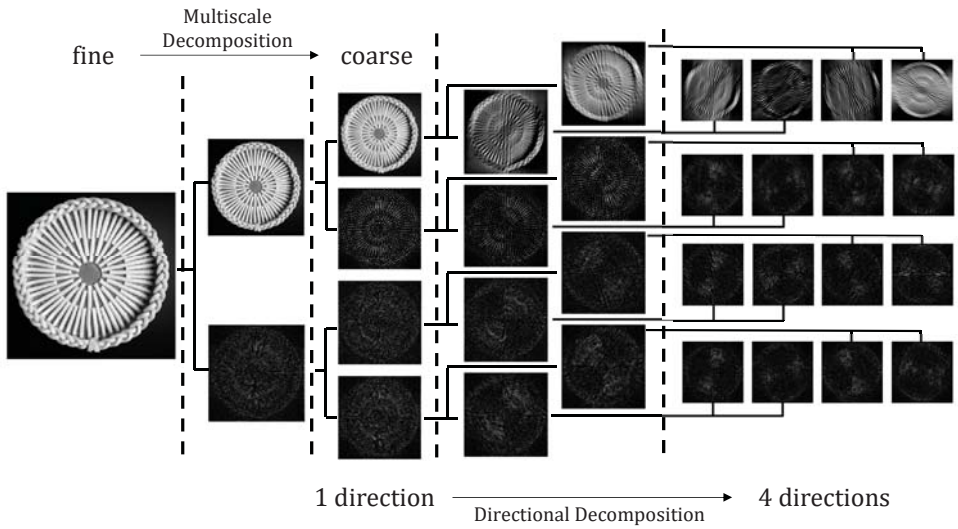

Figure 1: Illustration of multiscale directional decomposition provided by FBCN.

[9] emphasizes the inter-subband dependency while EBCOT [10] considers the intra-subband one. However, the intra- and inter-subband dependency are not sufficiently exploited in wavelet-based compression algorithms [11, 12]. Recently, end-to-end image compression schemes [13–16] leveraged CNNs to optimize information-theoretic parameters. Output feature maps are generated to by learned kernels to represent hierarchical information. Although this hierarchy is similar to subbands derived by conventional transforms, their dependencies can hardly be modeled. In [14], important coefficients were aggregated to improve coding performance with enhanced intra-subband dependency. Mentzer *et al.* [15] modeled the dependencies between feature maps with a 3D-CNN to serve as contexts for adaptive arithmetic coding (AAC). However, these CNN-based methods lack analysis on dependencies between feature maps and rely heavily on the estimation models.

In this paper, we propose an efficient subband coding framework for FBCN analysis coefficients, where intra- and inter-subband dependencies are jointly exploited with a SPIHT-like algorithm and subsequent primitive-based AAC. The SPIHT-like algorithm extends the spatial orientation tree for dependencies between subbands of different scales and directions. An information-theoretical measurement is introduced to formulate such dependencies. Consequently, primitive based adaptive arithmetic coding is developed to fit varying statistics of the generated bitstream for different lists and passes. Neural networks are leveraged to facilitate context-based prediction with non-linear estimation based on features from multiple sources, including scales, directions, spatial locations and significance of analysis coefficients. Experimental results show that the proposed framework improves the lossy coding performance for FBCN analysis coefficients in comparison to the state-of-the-arts subband coding schemes SPIHT.

The rest of this paper is organized as follows. Section 2 reviews multiscale and multidirectional image analysis with FBCN. Section 3 proposes the subband coding framework for the FBCN analysis coefficients, including SPIHT-like coding for inter-subband dependency and AAC primitives for intra-subband dependency. In Section 4,

an information-theoretic measurement is provided for the inter-subband dependency. Section 5 shows the experimental experiments for lossy image compression and Section 6 concludes this paper.

2 Multiscale Multidirectional Analysis with FBCNs

Multiscale decomposition is prevailing in lossy image compression [12, 17] for efficient progressive representations of images. To effectively capture the image contours, a series of directional filter banks have been developed to incorporate with multiscale decomposition. Filter bank based convolutional networks (FBCNs) [7, 8] achieve refined and efficient image analysis by cascading perfect reconstruction filter banks with convolutions along scale and direction dimension. FBCNs can be constructed by cascading layers of 1-D radial and directional filter banks in a flexible convolutional manner in the extended conjugate polar Fourier transform (ECPFT) domain. Here, the number of layers of radial and directional filter banks are denoted by l_1 and l_2. In fact, outputs would only depend on l_1 and l_2, but not affected by the orders of radial and directional decomposition. Thus, FBCNs are able to decompose an image into $2^{l_1+l_2}$ subbands by separately performing l_1-layer radial and l_2-layer directional analysis. In this paper, we utilize pairs of labels (r, d) to specify these subbands with scales $r = 1, \cdots, 2^{l_1}$ and directions $d = 1, \cdots, 2^{l_2}$. In summary, FBCN-based image compression methods can be distinguished from the CNN-based ones in the sense of learned kernels, nonlinear units and coefficient dependencies.

- FBCNs utilize manufactured filters for universal image analysis, while CNNs train localized kernels for specific tasks.
- FBCNs leverage orthogonal filters for *complete* representations, while CNNs employ nonlinear units (ReLU) for *overcomplete* ones.
- FBCNs allow explicit formulation of dependencies between coefficients of different subbands, while CNNs generate implicit feature maps.

3 Subband Coding Framework for FBCN Analysis Coefficients

Fig. 2 depicts the subband coding framework for FBCN analysis coefficients. Given FBCN analysis coefficients, a SPIHT-like algorithm is leveraged to model inter-subband dependencies with extended spatial orientation tree. Its generated bistream is composed of various lists of elements, which is adaptively encoded using well-designed primitives. Context-based prediction for arithmetic coding is improved with nonlinear estimation from neural networks, where multidimensional features are incorporated for enriched interdependencies in addition to correlations between neighboring bits. In the following subsections, we elaborate the SPIHT-like algorithm and primitive-based AAC.

SPIHT-like Algorithm for Inter-Subband Dependency

SPIHT algorithm contains two passes - significance pass and refinement pass. The inter-subband dependency is used in the significance pass by spatial orientation tree

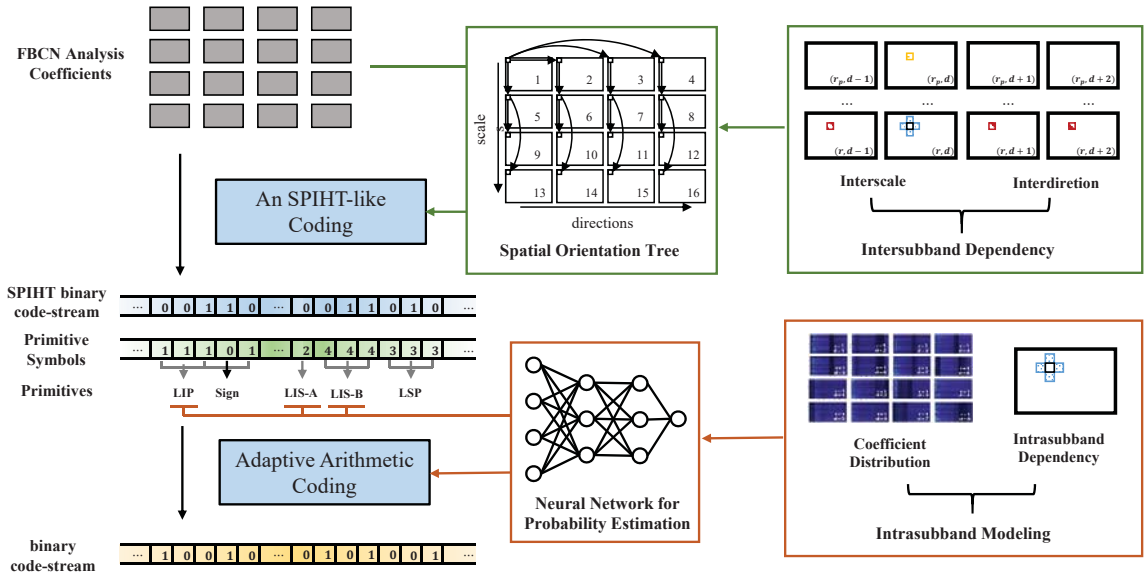

Figure 2: The proposed subband coding framework for FBCN analysis coefficients. A SPIHT-like algorithm is developed to formulate inter-subband dependencies with extended spatial orientation tree (SOT). Various lists of elements are generated based on the extended SOT for subsequent adaptive arithmetic coding. Multiple primitives are designed specifically for corresponding lists. Neural networks are leveraged to improve probability estimation with nonlinear prediction over multidimensional features indicating scales, directions, locations and significance of coefficients.

to transit the significant coefficients firstly. Since the FBCN analysis provides a directional multiscale representation, the inter-subband dependency is considered both in scales and directions. Thus, we extend the spatial orientation tree (SOT) to represent the dependencies between associated subbands with different frequencies and directions. Let us denote $\mathcal{O}(i,j,r,d)$ the set of offsprings of the analysis coefficient with the coordinate (i,j,r,d). Here, (i,j,r,d) means that this coefficient at the i-th row and j-th column in the subband of r-th scale and d-th direction. In Definition 1, we construct the extended SOT from the lowest subband with $r=1$ and $d=1$ in a recursive manner.

Definition 1 (Extended Spatial Orientation Tree) *Given FBCN with R radial layers and D directional layers, for arbitrary coefficient with coordinate (i,j,r,d), its set of offsprings $\mathcal{O}(i,j,r,d)$ in the extended spatial orientation tree is generated in a recursive manner.*

$$\mathcal{O}(i,j,r,d)=\begin{cases}\{(i,j,r,d+1),\ldots,(i,j,r,D),(i,j,r+1,d)\}, & r=d=1\\ \{(i,j,r+1,d)\}, & r=1,d>1\\ \{(i,j,2r,d),(i,j,2r+1,d)\}, & otherwise\end{cases}\tag{1}$$

According to Definition 1, parent-child pairs in the extended SOT represent varied mutual information between coefficients in subbands of different scales and directions. The recursive formulation in Eq. (1) is derived non-uniformly based on the

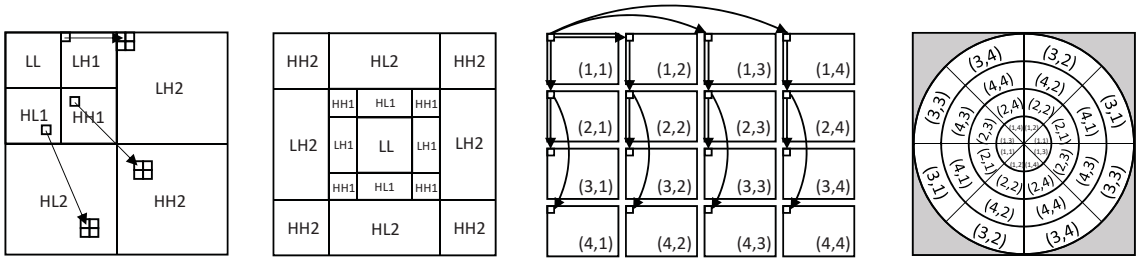

Figure 3: (a) Conventional spatial orientation tree of wavelet coefficients adopted in SPIHT; (b) Frequency partitioning in the Fourier transform domain corresponding to (a); (c) Extended spatial orientation tree of FBCN analysis coefficients. Subbands are associated according to their scales and directions; (d) Frequency partitioning in the Fourier transform domain corresponding to (c).

information-theoretic measurement of inter-subband dependency shown in Section 4. Specifically, subbands of the coarsest scale are organized by establishing the first direction as the parent of other directions. When the parent lies in the coarsest scale with $d = 1$, its 2^{l_2} children consist of one in the adjacent coarser scale with $d = 1$ and the ones for remaining $2^{l_2} - 1$ directions in the coarsest scale. However, there are only two children in the finer scales for the parent lying in the subband with $r > 1$. Fig. 3 illustrates the conventional SOT for wavelet coefficients and extended SOT for FBCN analysis coefficients. Since FBCN achieves a full decomposition on the radial and direction dimension, the extended SOT considers associations of subbands with different scales and directions.

Similar to SPIHT coding, list of insignificant signs (LIS) and list of insignificant pixels (LIP) are adopted to code the extended spatial orientation tree. Here, LIS and LIP are initialized with the coefficients of subband with $(r, d) = (1, 1)$. Thus, MN elements are required to initialize LIS/LIP for the subband of M-by-N FBCN analysis coefficients. Figure 4 illustrates the coarsest subbands of FBCN analysis coefficients for *Lena*, *Barbara* and *Baboon*. It shows that the significant coefficients are clustered in certain columns of these subbands. This fact would arise from the nonlinear transformation in preprocessing which contains oversampling of low frequency regions. The regular distribution of important coefficients implies that significant coefficients mainly appear in subbands with lower scale and their position information can be used in prediction and coding.

Primitive-based Adaptive Arithmetic Coding

Adaptive arithmetic coding is introduced to facilitate the coding performance of SPIHT-like algorithm for FBCN analysis coefficients, especially in low-bit rate region. Inspired by [17], five primitives are developed for context-based prediction of different elements in the two passes of binary code-stream generated by the SPIHT-like algorithm, e.g. the sign of significant coefficients and the value of encoding elements. For the significant pass, "LIS-A", "LIS-B" and "LIP" primitives are used to encode LIS and LIP, while "Sign" primitive is adopted for the sign of significant coefficients.

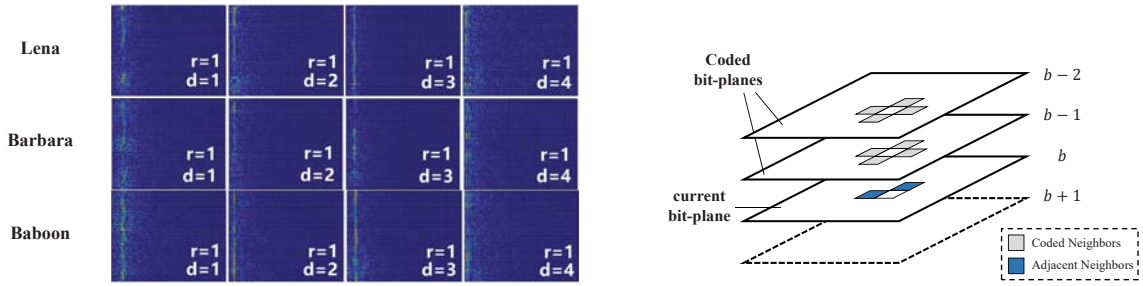

(a) (b)

Figure 4: Illustrative examples for neural network based context modeling. (a) Distribution of coefficients in lower-scale subbands of *Lena*, *Barbara* and *Baboon*; (b) Contexts for the bit to be encoded in current bit-plane.

The remaining "LSP" primitive is introduced in the refinement pass. Distinguishing contexts are derived during adaptive binary arithmetic coder for different primitives.

Furthermore, neural networks are adopted for context-based probability estimation in primitives for significant coefficients, i.e. "LIS-A", "LIS-B" and "LIP". It is rooted from the regular distribution of significant coefficients, as shown in Fig. 4(a). For each bit to be encoded, the proposed neural networks incorporates the varying information including its coordinate, significance of neighboring coefficients and encoded bits in the bit-plane to improve context-based prediction. To achieve nonlinear prediction and suppress overfitting, the neural networks are composed of a fully connected layer with ReLU activation function, a dropout layer and an activation layer using sigmoid function. Their parameters can be pretrained based on online available image datasets like ImageNet for a warm start.

In this paper, a 11-tuple vector is constructed as input features for each bit. For example, the coordinate (i, j, r, d, b) is selected to encode the b-th bit-plane of the (i, j)-th FBCN analysis coefficients in the (r, d)-th subband. Moreover, the significance of its four neighboring coefficients are adopted due to the smoothness in lower-scale subbands. To guarantee the causality of encoder, the upper and left neighbors of current bit are also leveraged to serve as contexts, as the scanning process is implemented in columns. Here, quantization is naturally achieved with the threshold $T = 2^b$ gradually varying with b to transit the significant coefficients into bit-planes. However, its can be further improved with sophisticated scheme like vector quantization.

4 Information-theoretic Measurement of Inter-subband Dependency

This section elaborates inter-subband dependencies between FBCN analysis coefficients, as the coding performance based on extended SOT tends to rely on the representation of inter-subband dependency. As mentioned in Definition 1, subbands are associated by jointly considering their scales and directions. This fact suggests that the inter-subband dependency can be evaluated in the sense of inter-scale and inter-direction correlations. To accurately formulate inter-subband dependencies, we

measure the mutual information of FBCN analysis coefficients in the pairs of associated subbands to evaluate their inter-scale and inter-direction correlations.

Definition 2 (Inter-subband Dependency) *Given the (r, d)-th subband X of FBCN analysis coefficients, its inter-subband dependency with subband Y is represented by their mutual information $I(X;Y)$.*

$$I(X;Y) = \sum_{1\le x\le L_X} \sum_{1\le y\le L_Y} P_{X,Y}(x,y) \log \frac{P_{X,Y}(x,y)}{P_Y(y)P_X(x)} \tag{2}$$

Here, $P_X(x)$ is the distribution of logarithms of coefficient values in X and the range of X is partitioned into L_x uniform intervals. $P_{X,Y}(x,y)$ is the joint distribution for X and Y.

According to Definition 2, when $Y = PX$ is the $(r-1, d)$-th subband, $I(X;PX)$ measures the inter-scale correlation, and $I(X;CX)$ for inter-direction correlation with subband $Y = CX$ with scale r. In practice, we estimate these correlations using $\hat{I}(X;PX)$ and $\hat{I}(X;CX)$ based on the empirical distributions of subband coefficients for given images. It is worth mentioning that $I(X;CX)$ is estimated with a sufficient statistic, as multiple subbands with the same scale would lead to "dilution" problem due to no sufficient number of samples. Thus, we estimate $I(X;T)$ instead of $I(X;X_1,X_2,\ldots,X_N)$ with the sufficient static $T = \frac{1}{N}\sum_{i=1}^{N}|X_i|$ of $X_1, X_2, \ldots, X_N$.

Table 1 compares the mutual information $\hat{I}(X;PX)$ and $\hat{I}(X;CX)$ by varying the scales and directions of subbands. It shows that the inter-scale and inter-direction correlations are comparable for subbands with lowest scales, while inter-direction correlations decrease with the growth of scale r. Consequently, we formulate the inter-subband using Eq. (1) and construct the extended spatial orientation tree.

5 Numerical Results

This section validates the proposed subband coding framework on natural images. We begin with the evaluation of inter-subband dependencies and primitive-based AAC for the proposed framework. Table 1 presents the estimated mutual information of subbands with $r = 1, 2, 7, 8$ and $d = 1, \cdots, 8$ in *Barbara* and *Lena*. Here, we only provide evaluation results of two test images due to the limitation of spaces, but similar results can be obtained for others. Table 1 shows that the inter-direction and inter-scale dependencies are significant for textured images, while the inter-directional dependencies descrease for higher scales in comparison to the inter-scale ones. Subsequently, we validate the primitives adopted for AAC. Table 2 shows that the proposed primitives improve code performance by about 16.24% and 9.09% in bit rates for *Barbara* and *Lena*, when compared with AAC using cumulative probability. Remarkably, the gains are consistent, especially in low bit-rate regions. Furthermore, rate-distortion performance is evaluated for lossy image compression, as shown in Figure 5. The proposed framework is compared with the state-of-the-art subband coding algorithms - SPIHT and SPIHT-AC (with AAC). For FBCNs, l_1 and l_2 are set 6 and 3. The dropout rate for neural networks is 0.5. In Fig. 5, rate-distortion curves in the low

Table 1: Mutual Information among Subbands

Barbara, $\hat{I}(X;PX)$									
r \ d	1	2	3	4	5	6	7	8	average
1	-	-	-	-	-	-	-	-	-
2	0.4221	0.3962	0.3264	0.3815	0.3706	0.3641	0.3512	0.3323	**0.3681**
7	0.3345	0.2935	0.3342	0.3187	0.3319	0.3075	0.2931	0.3088	**0.3153**
8	0.3483	0.3213	0.2860	0.2762	0.3405	0.2984	0.2428	0.3095	**0.3029**

Barbara, $\hat{I}(X;CX)$									
r \ d	1	2	3	4	5	6	7	8	average
1	0.4081	0.3993	0.3894	0.3847	0.3835	0.3858	0.3763	0.3807	**0.3885**
2	0.3695	0.3629	0.3264	0.3747	0.3481	0.3575	0.3700	0.3345	0.3555
7	0.3606	0.3167	0.2956	0.3163	0.3077	0.2856	0.2608	0.3219	0.3082
8	0.3147	0.2816	0.2793	0.2686	0.3534	0.3170	0.2462	0.2718	0.2916

Lena, $\hat{I}(X;PX)$									
r \ d	1	2	3	4	5	6	7	8	average
1	-	-	-	-	-	-	-	-	-
2	0.4032	0.3915	0.3357	0.3735	0.3982	0.3647	0.3103	0.313	**0.3221**
7	0.2929	0.3361	0.2465	0.2791	0.3718	0.3227	0.1813	0.1954	**0.2538**
8	0.2431	0.3081	0.2358	0.2695	0.3663	0.3013	0.2088	0.1978	**0.2416**

Lena, $\hat{I}(X;CX)$									
r \ d	1	2	3	4	5	6	7	8	average
1	0.4018	0.3945	0.3766	0.3885	0.3931	0.3845	0.3968	0.377	**0.3420**
2	0.3648	0.3778	0.3536	0.3576	0.3656	0.3524	0.2976	0.3278	0.3087
7	0.2795	0.2638	0.258	0.2851	0.2948	0.2745	0.2238	0.2447	0.2349
8	0.2669	0.2523	0.2628	0.2715	0.3017	0.2644	0.2481	0.2347	0.2335

bit-rate region are provided for *Lena*, *Barbara*, *Peppers* and *Plane*. It shows that the proposed framework outperforms other frameworks. The rate is measured by bit per pixel while the distortion is evaluated by Peak Signal-to-Noise Ratio (PSNR) of recovered images and original ones.

6 Conclusions

In this paper, we proposed a coding frame for a kind of manufactured convolutional network for the first time. The estimated inter-subband dependency inspired a spatial orientation tree for the SPIHT-like coding algorithm, and the probability involving intra-subband modeling promotes the performance of AAC.

Acknowledgment

This work was supported in part by the National Natural Science Foundation of China under Grant 61425011, Grant 61720106001, Grant 61529101, and in part by Shanghai High Technology Project under Grant 17511106603 and the Program of Shanghai Academic Research Leader under Grant 17XD1401900.

Table 2: Performance Comparison with/without Primitives

Barbara				*Lena*			
w/(bpp)	w/o(bpp)	PSNR	Gain	w/(bpp)	w/o(bpp)	PSNR	Gain
0.0113	0.0130	15.30	-12.97%	0.0138	0.0152	15.66	-8.84%
0.0222	0.0267	15.58	-16.79%	0.0329	0.0373	21.24	-11.58%
0.0504	0.0617	18.53	-18.30%	0.0589	0.0658	22.86	-10.39%
0.0592	0.0726	18.75	-18.44%	0.0894	0.0978	23.54	-8.59%
0.0854	0.1048	19.44	-18.52%	0.1252	0.1400	24.29	-10.56%
0.1136	0.1387	19.93	-18.12%	0.1690	0.1861	25.03	-9.18%
0.1528	0.1863	20.25	-17.99%	0.1957	0.2143	25.64	-8.70%
0.1966	0.2317	20.38	-15.14%	0.2220	0.2416	26.08	-8.11%
0.2123	0.2519	21.08	-15.72%	0.2588	0.2794	26.40	-7.37%
0.2238	0.2692	21.36	-16.86%	0.2946	0.3191	26.53	-7.70%
0.2504	0.2985	21.72	-16.12%	0.3331	0.3688	26.81	-9.67%
0.2821	0.3302	21.87	-14.55%	0.3692	0.4049	27.15	-8.81%
0.3168	0.3669	21.92	-13.65%	0.4091	0.4463	27.41	-8.34%
0.3555	0.4224	22.35	-15.84%	0.4443	0.4920	27.54	-9.71%
0.3954	0.4625	22.61	-14.52%	0.4847	0.5318	28.01	-8.86%

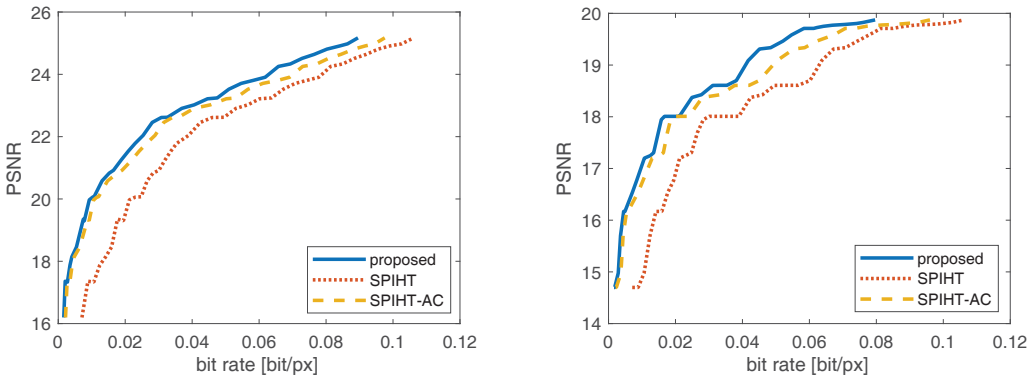

(a) *Lena* (b) *Barbara*

(c) *Peppers* (d) *Plane*

Figure 5: Rate-distortion curves for *Lena*, *Barbara*, *Peppers* and *Plane*.

References

[1] Alex Krizhevsky, Ilya Sutskever, and Geoffrey E Hinton, "Imagenet classification with deep convolutional neural networks," in *Advances in Neural Information Processing Systems*, 2012, pp. 1097–1105.

[2] Karen Simonyan and Andrew Zisserman, "Very deep convolutional networks for large-scale image recognition," *arXiv preprint arXiv:1409.1556*, 2014.

[3] Kaiming He, Xiangyu Zhang, Shaoqing Ren, and Jian Sun, "Deep residual learning for image recognition," in *Proceedings of the IEEE Conference on Computer Vision and Pattern Recognition*, 2016, pp. 770–778.

[4] Joan Bruna and Stéphane Mallat, "Invariant scattering convolution networks," *IEEE Transactions on Pattern Analysis and Machine Intelligence*, vol. 35, no. 8, pp. 1872–1886, 2013.

[5] Stéphane Mallat, "Group invariant scattering," *Communications on Pure and Applied Mathematics*, vol. 65, no. 10, pp. 1331–1398, 2012.

[6] Thomas Wiatowski and Helmut Bölcskei, "A mathematical theory of deep convolutional neural networks for feature extraction," *IEEE Transactions on Information Theory*, vol. 64, no. 3, pp. 1845–1866, 2018.

[7] Can Xu and Hongkai Xiong, "Revertible deep convolutional networks with iterated directional filter bank," in *Proceedings of the IEEE International Conference on Acoustics, Speech and Signal Processing (ICASSP) 2016*. IEEE, 2016, pp. 1586–1590.

[8] Can Xu, Wenrui Dai, and Hongkai Xiong, "Extended conjugate polar fourier transform in convolution network," in *Proceedings of the IEEE International Conference on Image Processing (ICIP) 2017*. IEEE, 2017, pp. 2453–2457.

[9] Amir Said, William A Pearlman, et al., "A new, fast, and efficient image codec based on set partitioning in hierarchical trees," *IEEE Transactions on Circuits and Systems for Video Technology*, vol. 6, no. 3, pp. 243–250, 1996.

[10] David Taubman, "High performance scalable image compression with ebcot," *IEEE Transactions on Image Processing*, vol. 9, no. 7, pp. 1158–1170, 2000.

[11] Ramin Eslami and Hayder Radha, "Wavelet-based contourlet transform and its application to image coding," in *Proceedings of the IEEE International Conference on Image Processing (ICIP) 2004*. IEEE, 2004, vol. 5, pp. 3189–3192.

[12] Jingyu Yang, Yao Wang, Wenli Xu, and Qionghai Dai, "Image coding using dual-tree discrete wavelet transform.," *IEEE Transactions on Image Processing*, vol. 17, no. 9, pp. 1555–1569, 2008.

[13] Johannes Ballé, Valero Laparra, and Eero P Simoncelli, "End-to-end optimized image compression," *arXiv preprint arXiv:1611.01704*, 2016.

[14] Oren Rippel and Lubomir Bourdev, "Real-time adaptive image compression," *arXiv preprint arXiv:1705.05823*, 2017.

[15] Fabian Mentzer, Eirikur Agustsson, Michael Tschannen, Radu Timofte, and Luc Van Gool, "Conditional probability models for deep image compression," in *Proceedings of the IEEE Conference on Computer Vision and Pattern Recognition (CVPR)*, Salt Lake City, UT, USA, 2018, pp. 4394–4402.

[16] Zhengxue Cheng, Heming Sun, Masaru Takeuchi, and Jiro Katto, "Deep convolutional autoencoder-based lossy image compression," *arXiv preprint arXiv:1804.09535*, 2018.

[17] David Taubman and Michael Marcellin, *JPEG2000 Image Compression Fundamentals, Standards and Practice: Image Compression Fundamentals, Standards and Practice*, vol. 642, Springer Science & Business Media, 2012.